

Recent changes in total ice volume on Volcán Villarrica, Southern Chile

Andrés Rivera · Rodrigo Zamora · José Uribe · Anja Wendt · Jonathan Oberreuter · Sebastián Cisternas · Fernando Gimeno · Jorge Clavero

Received: 3 October 2013 / Accepted: 13 June 2014

© The Author(s) 2014. This article is published with open access at Springerlink.com

Abstract Results obtained by the first intensive airborne surveys carried out at Volcán Villarrica (39°S) in Southern Chile, are presented. These campaigns included the use of a scanner laser system, for detecting the glacier surface topography, and a helicopter-borne ice penetrating radar, for measuring ice thicknesses. These surveys allowed determining the snow and ice volume storage at this volcano, volume which is susceptible to melt during eruptive events generating dangerous fast flows (lahars). Volcán Villarrica is one of the most active volcanoes in Chile, with frequent eruptive events, many of them associated with lahars which are considered the most hazardous process at this volcano. In fact, most of the casualties and infrastructure damages incurred during historical eruptive events at the volcano are associated with lahars. With use of the radar and laser data, a total volume of $1.17 \pm 0.1 \text{ km}^3$ of water equivalent (w.eq.) at the volcano in 2012 was calculated, only 37 % of the estimated volume of 1961, a reduction mainly explained by the area shrinkage and ice thinning rates observed in the last 51 years. This total volume represents a lower boundary available for melting during eruptive events when lahars mudflows can be generated, because mainly in the winter, nearly 0.14 km^3 w.eq. are potentially added to the volcano as temporal snow falls. The volume of water equivalent lost in recent decades does not mean a lower risk associated with these flows, as there has been a huge increase in populated areas in the surroundings of the volcano in recent years.

A. Rivera (✉) · R. Zamora · J. Uribe · A. Wendt · J. Oberreuter · S. Cisternas · F. Gimeno
Centro de Estudios Científicos (CECs), Valdivia, Chile
e-mail: arivera@cecs.cl

A. Rivera
Departamento de Geografía, Universidad de Chile, Santiago, Chile

A. Wendt
Bavarian Academy of Sciences, Munich, Germany

J. Clavero
Escuela de Geología, Universidad Mayor, Santiago, Chile

Keywords Ice-capped volcanoes · Volcanic risk · Airborne radar · Lahar

1 Introduction

Several active volcanoes in the Southern Volcanic Zone (36–46°S) of Chile are partially ice capped (Stern et al. 2007). During eruptive events most of these glaciers are susceptible to rapid melting, and resulting volcanic mudflows (lahars) are frequently generated causing infrastructure destruction and casualties, this process being one of the main volcanic hazards in the region (Naranjo and Moreno 2004; Clavero and Moreno 2004; Moreno and Clavero 2006; Moreno 2000; Castruccio et al. 2010). In spite of the importance of these glaciers located on active volcanoes, little is known about the volume of water equivalent storage and about their recent behavior in response to climate change (Rivera and Bown 2013). Based upon recent glaciological research, we know the glaciers are experiencing negative glacier mass balances (Rivera et al. 2005) and, as a consequence, generalized frontal retreats are taking place (Rivera et al. 2012). Few scientific studies are available concerning ice thicknesses and precise surface topography on ice capped volcanoes. Among these are Gilbert et al. (1996), regarding Nevados de Sollipulli, and Rivera et al. (2006) concerning Villarrica and Mocho-Choshuenco volcanoes.

In view of the associated risks of ice and snow on active volcanoes, recent studies (Castruccio et al. 2010) have tried to estimate water-equivalent from ice melting during eruptive events by studying lahar deposits and modeling the amount of water available at the lahar inception areas. This modeling effort however, requires validation obtained from direct ice thickness measurements. Obtaining more accurate ice volumes at individual lahar valleys will certainly help to better constrain the hazardous areas associated with this type of flow and therefore better estimate the associated risk.

The progressive replacement of discrete gravimetric data (containing >20 % errors (Casassa 1987)) with data acquired by radio echo sounding systems (Watts and England 1976), used with different ground configurations (Rivera et al. 2001), has significantly improved our knowledge about the ice thickness of Chilean glaciers in recent decades. These surveys had limited spatial coverage due to the difficulties of acquiring on-foot measurements while walking along crevassed, steep and rough glacier ablation areas. The accumulation areas were better surveyed by using skidoos along smooth snow surfaces, but they utilized low frequency radar systems (2–10 MHz) and the relatively low power of the transmitters, made them incapable of detecting thicknesses of more than 600 m of temperate ice (Rivera and Casassa 2002).

During recent years, a number of CECs (Centro de Estudios Científicos) surveying capabilities improvements have been implemented, including among others, a new airborne radar system (Zamora et al. 2009). In spite of the success of this new system, the maximum penetration ranges did not significantly improve, only detecting up to 670 m of ice in temperate ice (Zamora et al. 2009), and the logistical constrains of flying with a long antenna system (150 m) behind airplanes precluded a safe operation over steep glaciers.

In order to enhance the penetration range capabilities and provide a safe logistic operation, a new helicopter-borne radar system was recently designed and tested by CECs. This paper includes the recent results obtained by this new impulse radar system using a hanging bow-tie dipole antenna working at a central frequency of 20 MHz.

1.1 Study area

Volcán Villarrica ($39^{\circ}25'S/71^{\circ}56'W$, 2847 m asl Fig. 1) is one of the most active volcanoes in the Chilean Andes (Lara 2004) with eruptive activity in historical times characterized by mild strombolian processes (Naranjo and Moreno 2004), permanent degassing and periodic explosions (Witter and Delmelle 2004). The volcano has an almost permanent lava lake within the crater, which has remained oscillatory since the end of the 1984–1985 eruption, between 90 and 180 m below the crater surface rim (Calder et al. 2004; Witter and Delmelle 2004). Its historical eruptive activity indicates high frequency of mild explosive eruptions, VEI between 3 and 4 (Volcanic Explosivity Index, VEI, Newhall and Self (1982)) with more than 500 eruptive events since 1558 (Petit-Breuilh and Lobato 1994), and tens of more explosive eruptions (VEI 3 to 6) recorded in pre-historical times, including two large ignimbrite-forming eruptions in the Late Pleistocene and Holocene (13.7 and 3.7 ka BP; e.g. Clavero and Moreno (2004)).

The most recent violent eruption took place in 1971–72 when lava flows were generated, as well as 30 to 40 km/hr lahars that flew down towards Lagos Villarrica and Calafquén (Naranjo and Moreno 2004). During the first stage of the 1971–1972 eruptive cycle, lava fountaining poured out from a NNE fissure on the upper flanks of the volcano generating rapid melting of the glaciers (González-Ferrán 1995), both towards the northern and southwestern flanks of the edifice, where the main lava flows were distributed (Moreno and Clavero 2006). Lahars produced by the eruptions of Volcán Villarrica in 1948–1949, 1963–1964, and 1971–1972 have produced more than 75 casualties (Stern 2004), and therefore lahars are considered to be the main hazard of the volcano (Moreno 2000). The main lahar channels descending from the volcano glaciers (Figure 1) have been mapped and their deposit characteristics studied by Castruccio et al. (2010). Castruccio (2008) has also modeled the possible extent of lahars in the main drainages around the volcano for different scenarios, according to volcanological and the available glacier data.

The main ice cap at the volcano can be divided into several glacier tongues, which are mainly flowing toward the south and north–eastern sides, where partially debris-ash covered Glaciar Pichillancahue-Turbio is located (Fig. 2). This glacier partially infills a volcanic caldera depression (Clavero and Moreno 2004) probably associated with two partial collapses of ancestral edifices that occurred in Late Pleistocene to Holocene times. The other glacier tongues of the volcano were more difficult to be delineated due to surface topography complexity.

The energy balance of Glaciar Pichillancahue-Turbio has been monitored since 2003 (Brock et al. 2007), and Global Positioning System (GPS) as well as digital photography measurements have been carried out since 2005 (Rivera et al. 2008). A couple of on-the-ground ice thickness surveys are also available (Casassa et al. 2004; Rivera et al. 2006). However, these measured tracks may not be representative of the whole glacier, as surveys were only conducted above the Equilibrium Line Altitude (ELA), approximately located at 2000 m asl (Rivera et al. 2006).

Considering the lack of a comprehensive surface and subglacial topography data set for the whole ice cap, a new airborne survey of Volcán Villarrica was carried out in January (LIDAR) and April 2012 (Radar), with the main aim of surveying the surface topography, testing a new helicopter-borne radar able to penetrate temperate ice, and measuring the most crevassed and inaccessible areas of the volcanoes glacier.

This paper describes the methods, surveys and main results obtained in recent years, providing the most updated and accurate estimation of the water equivalent volume storage

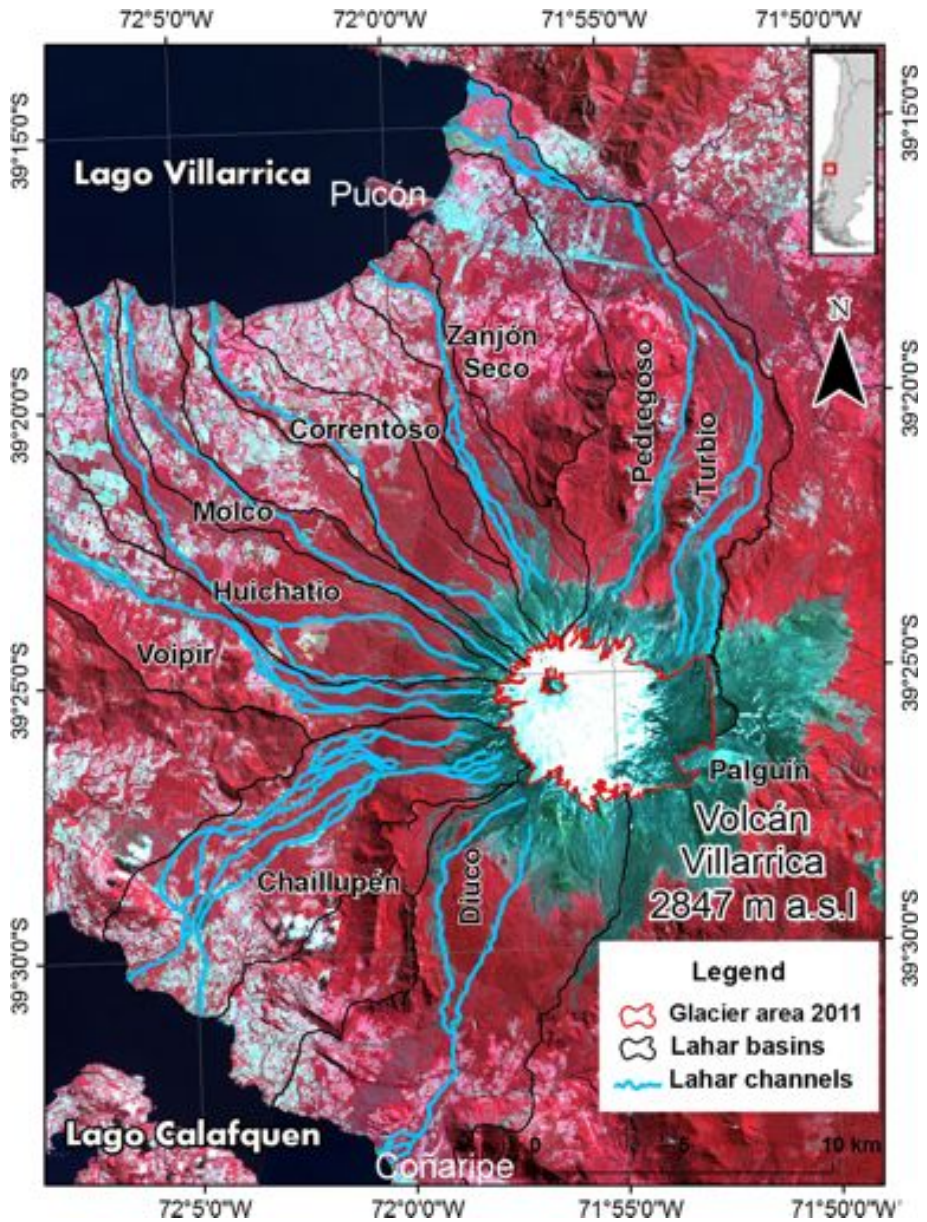


Fig. 1 Location map, where the nine main lahar basins are labeled. The background is a false colour composite ASTER bands 3, 2 and 1 shown as R, G and B acquired on February 26, 2011. The lahar channels in blue have been mapped from Castruccio et al. (2010). In black, the glacier basins associated with these lahars. In red, the glacier boundary

on the ice cap, which was divided among the main glacier basins feeding the most frequent lahar channels in the area. The resulting data are also used for better constrain specific volcanic hazards.

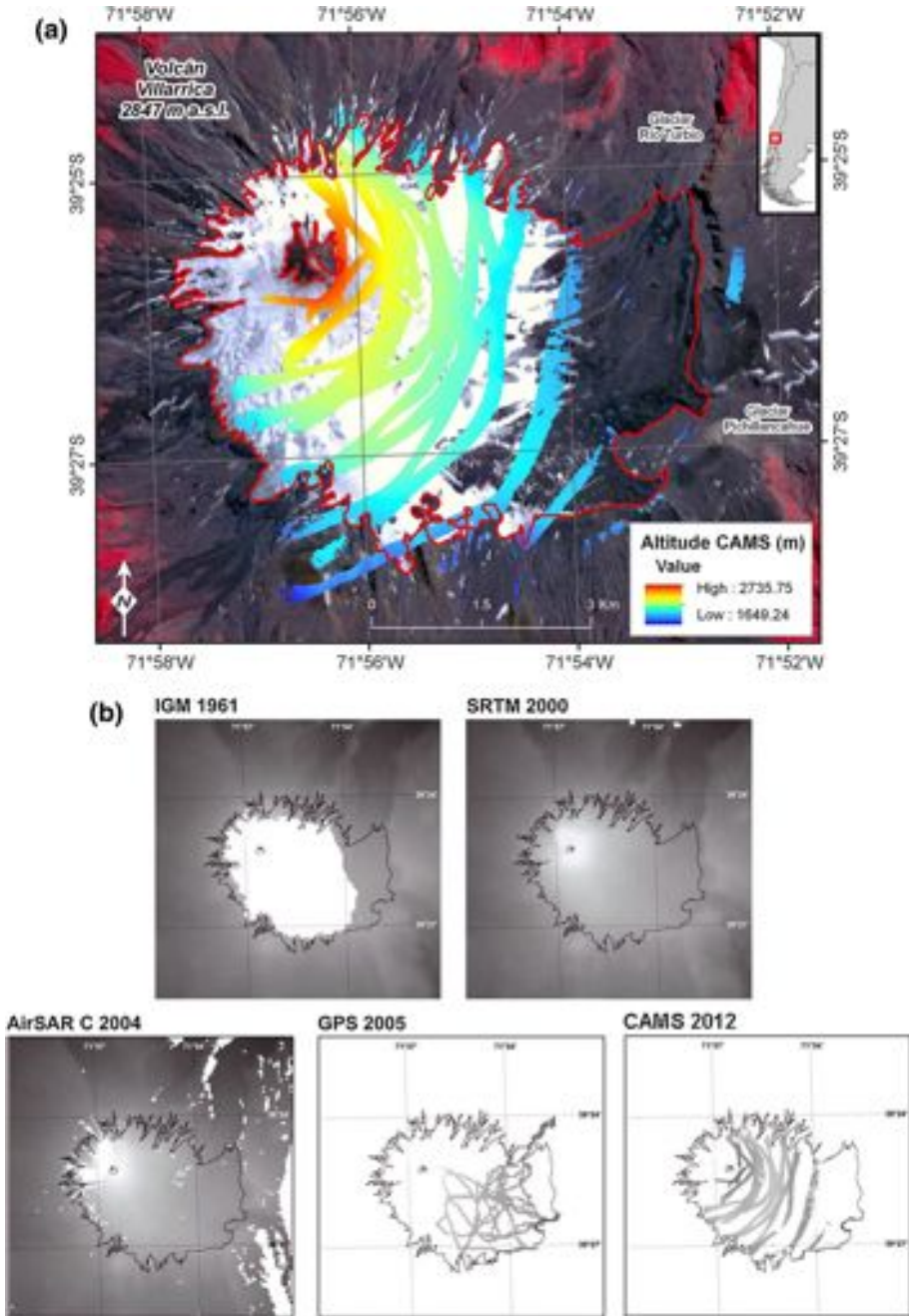


Fig. 2 **a** Surface topography measured by the CEMS LIDAR system (CEMS) in January 2012. The background is a false colour composite ASTER 321 acquired on February 26, 2011. **b** Available surface topography data sets coverage (see Table 3 for more details). The white areas imply no data

2 Data and methods

2.1 Previous topographic data sets

The first regular topographic map of the volcano was produced by the Chilean Military Geographical Institute (IGM) from aerial photographs acquired on 12 December 1961. The contour lines interval was 25 m, and the vertical error was estimated to reach 18 m. The main problem of this topographic map, however, is the lack of stereoscopic vision on the aerial photographs at the ice-capped area, precluding glacier topography determination for most of the glacier (Rivera et al. 2006).

Shuttle Radar Topography Mission (SRTM) data collected in February 2000 by NASA and the US Department of Defense produced a 90m grid size Digital Elevation Model (DEM) with a vertical accuracy of 7–10 m (Rignot et al. 2003). This data covered almost the whole volcanic cone, with minor gaps at the steepest flanks.

In March 2004, a Jet Propulsion Laboratory airborne synthetic aperture radar (AirSAR-C) was used to survey the topography of the volcano, yielding a 10 m pixel size DEM with an estimated vertical error of 6 m (Rivera et al. 2006).

In 2005, on-the-ground geodetic quality GPS receivers were used to measure several profiles in the ablation zone of the glacier resulting in vertical accuracies of 0.2 m in localized areas (Rivera et al. 2008).

2.2 First airborne LIDAR survey

The principal component of the CECs Airborne Mapping System (CAMS) is an airborne laser scanner RIEGL LMS-Q240-60 with a wave length of 904 nm and a scan angle of 60 °C which allows the measurement of distances within a maximum range of 500 m and a vertical accuracy of 20 cm. For the georeferencing of the laser measurements, the system is equipped with an Inertial Measurement Unit (IMU), IMAR iNAV-FMS AIRSURV, and a dual-frequency GPS receiver Javad Legacy with a JNS AvAnt antenna. The system is completed by an SLR camera Canon EOS5D and -depending on the mission- a thermal infrared Forward-looking imaging system camera. At the Villarrica survey, the system was mounted on a Piper PA-30 Twin Comanche airplane. A GPS reference station was installed and operated at the Temuco Maquehue airfield (38°45'S/72°38'W, 114 m asl), located 90 km away (W) from Volcán Villarrica's summit, enabling differential post processing of the aircraft GPS data and ensuring a short baseline during IMU alignment.

A calibration flight mission was performed immediately after takeoff, including a two-turn clover-like track over the Temuco airfield in order to determine eccentricities between the different instruments that vary with every installation. The flight track lines at Volcán Villarrica were designed to follow the most recurrent lahar channels in historical times (Castruccio et al. 2010) and covered most of Glaciar Pichillancahue-Turbio. However, the abrupt slopes prevented completion of surface topography coverage, especially in the upper part of the main cone (Fig. 2).

The first step of the data post processing involved combining analysis of GPS and IMU measurements to generate the survey trajectory using the Waypoint Inertial Explorer software. This trajectory was then used to transform the laser measurements into geographic coordinates (WGS-84). The resulting point cloud was processed in the TerraSuite software package for calibration, filtering and production of a final data set (LIDAR-2012) that was characterized by 0.5 points per square meters and horizontal/vertical errors in the order of 0.5 m. This cloud was then rasterized through an aggregation procedure to produce

a DEM with different pixel sizes, depending on the resolution of the previous coarser data sets (e.g. SRTM has 90 m) used for comparison purposes.

The comparison between available data sets allowed for the estimation of ice elevation changes in recent years. This comparison also made it possible to produce a better than 90 m pixel size DEM (SRTM) for the whole volcano. The idea was to use, as a base line, the best and most recent data set (LIDAR 2012), and for glacier areas not covered by this data (40 %) to use the other available data sets (Rivera et al. 2006), which were previously corrected by the estimated ice elevation changes during the intervening periods. The resulting surface DEM is comprised of LIDAR-2012 data (50 %), adjusted GPS data from 2005 (15 %), adjusted AirSar-C data from 2004 (25 %) and adjusted SRTM data (10 %). A pixel size of 10 m was chosen and the resulting vertical accuracy is estimated to be near 5 m. Here, the estimated error is the combined error of all available data sets used to compile the final DEM. The 5 m accuracy was calculated taking into account the individual errors (Table 3) and the spatial coverage of each data set.

2.3 Previous ice thickness data

In 2003, several on-the-ground penetrating radar short profiles (200 m long) were measured on the northern flank of the volcano. An Ohio State University (USA) transmitter working at a central frequency of 5.6 MHz was used. These surveys resulted in a maximum thickness of 112 m and mean of 47 m with an estimated accuracy of 15 % (Casassa et al. 2004).

A maximum thickness of 195 m with a mean thickness of 75 m was obtained in a more extensive on-foot survey performed in January 2005, on the northeastern glacier of the volcano. This survey used an on-the-ground radio echo sounding system, comprised of a University of Bristol (UK) transmitter with a pulse amplitude of 800 Vpp (Gilbert et al. 1996) and resistively loaded antennae with a central frequency of 5 MHz based upon a model by Watts and Wright (1981). In several segments of the surveyed tracks the sub-glacial topography was either not visible or was obscured due to internal ash/debris layer related noise and due to the presence of large crevasses. The ablation zone was only partially measured due to the rough surface topography and the presence of crevasses which limited personnel movement on the ground. The accuracy of these data was estimated to be between 5 and 10 % of the total ice thickness (Rivera et al. 2006).

2.4 First helicopter borne radar survey

Previous successful helicopter-borne data obtained on temperate, polythermal and cold ice (Kennett et al. 1993), allowed CECs together with the German Federal Institute for Geosciences and Natural Resources (BGR) in Hannover, and the Chilean private company Unmanned, to develop a new radar system aiming to survey temperate ice in Chile using helicopter support.

This new radar system has a 3.2 kV impulse transmitter with a central frequency of 20 MHz and a pulse repetition frequency set at 3 kHz. The receiver operates a 20 MHz of bandwidth with a low noise amplifier of 20 dB, averaging 256 traces and a sample frequency rate of 400 MSPS (Megasamples Per Second). It has a density of 8,192 14-bit samples per trace, and a time range of 20 μ s.

The antenna is an aluminium structure of 7 \times 5 \times 1 m dimensions, weighing near to 400 kg. The antenna hangs at 20 m below the helicopter, and is connected to a portable rough computer by an optical fibre cable. The antenna is fitted with a radar transmitter,

previously described. The radar receptor is equipped with two channels at a low and a high gain, with digital step attenuators for gain adjustment; and a pointing laser altimeter system measuring the distance between the system and the glacier/ground surface.

Dual frequency JNS Lexon GD GPS receivers were used to georeference all measurements, using one base station with a MarAnt GD antenna at the Villarrica airfield (9 km away from the volcano's summit) and a second receiver installed at the radar antenna. Data post processing was done using the commercial software package GrafNav providing trajectories of the radar antenna with a better than 1 m accuracy. An IMU Xsens MTi-G was tied to the GPS receiver located at the radar antenna, providing attitude for each of the measurements. Taking the positioning and attitude errors into account, the radar data positioning error on the ground was estimated to be <5 m.

The radar measurements were acquired using a Bell 407 helicopter, flying at near 40 m above the glacier surface, at 40 knots air speed. The survey was conducted along pre-designed tracks covering most of the glaciers, including longitudinal and transversal profiles previously measured in 2005 (Rivera et al. 2006) for comparison purposes.

Due to the total antenna weight, the helicopter could only fly during stable weather conditions, when a 40 m altitude should be maintained in order to collect useful data. However, even during good flying conditions, the presence of steep slopes or rough surface glacier topography (crevasses) complicated the data acquisition, because the helicopter couldn't maintain the needed altitude above the ground, reducing the radar signal capacity to penetrate the underlying ice.

The radar data were analysed using software developed by CECs as well as REFLEXw (Sandmeier 2004), with which two-way travel times and amplitudes of the reflection wave were determined using a wave propagation velocity for temperate ice of 168 m/ μ s (Macheret et al. 1993). A mean subtraction of a dewow filter, bandpass butterworth filter, background removal, migration and adjustment of the gain function were applied to the raw data. Occurring at constant time delays, the reflections coming from the helicopter were removed using a static correction. Ice thicknesses were obtained by on-screen digitalization of the migrated and filtered radargrams. The positioning of each trace within these radargrams was determined by the time synchronicity between the GPS and Radar clocks. The resulting ice thickness vector files were exported into a Geographical Information System (GIS) software where glacier surface heights for each data point were assigned from the DEM produced by all available data sets described previously.

2.5 Water equivalent at the volcano

The resulting ice thickness data point cloud was compiled in GIS commercial software, and rasterized into a 90 m pixel size grid. These pixels were interpolated to determine the total ice volume at the volcano using an Inverse Distance Weighted method (Schloeder et al. 2001). The outline of the glacier was also used in the interpolation, assuming a border ice thickness value of 5 m. In areas where the radar coverage was scarce, a mask was used to avoid extrapolations without ground control. In total, the ice thickness DEM covered 88 % of the total glacier area with a 90 m pixel size. Only the western flank of the volcano was not interpolated and an average value was assigned to these basins.

To estimate the volume of water equivalent stored at the volcano, the pixel area was multiplied by the ice thickness value of each cell of the resulting DEM. In order to convert this ice volume into water equivalent, a mean density of 0.8 gr/cm³ was used. This density is close to 10 % smaller than the theoretical ice density value (Paterson 1994). This lower

density value was used because of the presence of debris-ash covered areas, and temporal snow and firn. This snow layer is however minimal (a few meters) because the radar survey took place at the end of the summer when the Accumulation Area Ratio (AAR) reaches 0.38 (Rivera et al. 2011), and therefore, melting is taking place on most of the glacier, explaining its temperate conditions (Rivera et al. 2006).

In order to better estimate the lahar hazards associated with the ice volume at this active volcano, the ice cap must be divided into glacier basins from which the lahars can be originated. Defining the ice divides at a volcanic edifice such as Villarrica is difficult because the surface topography is complex and the ice flow lines and lower tongues are not easily delineated. However, with the most accurate and detailed DEM, 9 main glacier basins were delineated. These basins are not necessarily defined by ice flow as traditionally done in glaciology (Paterson 1994). In our case, different glacier basins were joined depending on the lahar channels mapped thanks to the historical record available for the volcano (Naranjo and Moreno 2004; Castruccio et al. 2010). For example, Glaciar Turbio is the most easily delineated basin using the traditional glaciological approach, however in this case, the neighbouring basin to the west was merged, because the lahars coming from these two areas (Pedregoso and Turbio) form a single lahar path at low altitude (Fig. 1).

3 Results

3.1 Areal changes

The glacier area on Volcán Villarrica has undergone a continuous reduction since 1961, when the first aerial vertical photograph was obtained. The area shrinkage rates are not constant, as in the first period (1961–1976) the total area reduction was maximum (Table 1), then the glacier was relatively stable for the period 1976–1986, reaching higher reduction rates in the last decade. Also, area losses are not taking place at the same rate everywhere around the cone, as Glaciar Pichillancahue (Fig. 2a) began to retreat at higher rates in the last decade, whilst Turbio experienced the maximum rate at the end of the 1990s (Table 2). In total, the glacier area at Volcán Villarrica in 2011 is only 71 % of the 1961 area, reduction mainly observed at the Pichillancahue tongue and at the southern edge of the ice cap (Rivera et al. 2008). The northern flank of the cone also experienced an area reduction, which could be related to the lava flow paths of the last eruptions (1971 and 1984) that eroded the glacier on this side.

3.2 Surface topography and ice elevation changes

Ice elevation changes measured at the ice cap fluctuated between -0.48 and -1.03 m/a (Table 3). Maximum thinning was observed between 2005 and 2012, when the most accurate combined data set is available (± 0.05 m/a). The spatial distribution of the elevation changes during this period (Fig. 3), does not follow the typical curve with the highest thinning at the lower parts of the ablation areas, reaching smaller thinning or no changes at the accumulation area (e.g. Rignot et al. 2003). The ablation zone is shown to have experienced mainly negative elevation changes, comprising of very few values with thickening ($+0.2$ m/a), and most of the pixels with a maximum thinning of near 3 m/a.

Overall, the ablation zone experienced an average elevation change of -1.08 ± 0.05 m/a, whilst the accumulation area (above 2,000 m asl), where changes are increasingly more homogeneous with elevation, experienced an average elevation change of -0.95 ± 0.05 m/a.

Table 1 Glacier area changes since 1961

| Data set | Acquisition date | Glacier area (km ²) | Days since IGM | Δ (km ² /a) | % of 1961 | Source area |
|--------------|------------------|---------------------------------|----------------|-------------------------------|-----------|------------------------|
| IGM | 12-12-1961 | 39.9 | – | – | 100 | Rivera (1989) |
| LANDSAT MSS | 08-02-1976 | 36.3 | 5171 | –0.25 | 91 | This study |
| LANDSAT 5 TM | 15-02-1986 | 35.6 | 8831 | –0.18 | 89 | |
| ASTER | 02-24-2007 | 30.1 | 16510 | –0.22 | 75 | Rivera and Bown (2013) |
| ASTER | 26-02-2011 | 28.3 | 18187 | –0.23 | 71 | This study |

Table 2 Glacier frontal changes in m/a (this study)

| Period | Frontal change (m/a) | |
|-----------|------------------------|----------------|
| | Glaciar pichillancahue | Glaciar turbio |
| 1961–1976 | –29 | |
| 1976–1983 | –26 | –15* |
| 1983–1987 | –19 | –15 |
| 1987–1998 | –37 | –19 |
| 1998–2003 | –53 | –139 |
| 2003–2005 | –60 | stable |
| 2005–2007 | –54 | –33 |
| 2007–2011 | –31 | –19 |
| 1961–2011 | –29 | –22 |

* 1961–1983

Table 3 Ice elevation changes between CECs LIDAR (CAMS) and other data sets

| Data set | Acquisition date | Vertical error per data set (m) | Compared area (km ²) | Days since CAMS | Δ (m/a) | Combined RMS |
|----------|------------------|---------------------------------|----------------------------------|-----------------|----------------|--------------|
| IGM | 12-12-1961 | 18 | 2.23 | 18294 | –0.95 | 0.36 |
| SRTM | 09-02-2000 | 10 | 14.68 | 4356 | –0.62 | 0.83 |
| AIRSAR | 20-03-2004 | 6.2 | 10.26 | 2855 | –0.48 | 0.79 |
| GPS | 05-01-2005 | 0.2 | 0.12 | 2564 | –1.03 | 0.05 |
| CAMS | 13-01-2012 | 0.5 | – | – | – | – |

The high scattering of elevation change values in the ablation zone could be related to the hummock-like roughness topography produced by the differential ablation that takes place at this debris-covered area (Rivera et al. 2008). In this case, elevation changes could be very different depending on whether the survey is done at the top or bottom of each hummock or pyramid-like prevailing form. These hummocks have steep flanks, with differences in height between bottom and top ranging from less than 1 meter to 5 meters approximately. The more homogeneous elevation changes observed at the accumulation area are probably related to the steeper but smoother flanks of this mainly snow-covered area.

The long term elevation change rate (–0.95 m/a) was calculated by the comparison of areas where the stereoscopic vision of the 1961 aerial photographs allowed IGM to produce a cartography. These sectors are at the lower part of the ablation areas, and therefore the

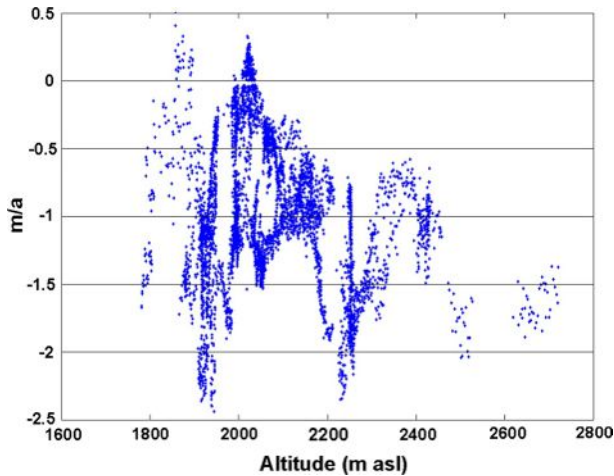


Fig. 3 Ice elevation changes (m/a) between 2012–2005 (LIDAR minus GPS data), versus altitude (m asl)

thinning rate must be considered with care, because it probably represents a maximum rate not representative of the whole glacier.

No clear elevation change trend was detected when all available data sets were compared, however, when 1961 data set was subtracted from the SRTM data (year 2000) an elevation change of -0.69 ± 0.54 m/a was revealed (Rivera et al. 2006), a much smaller thinning rate compared with the results obtained here between 2005 and 2012.

3.3 Ice thickness and volume of water equivalent

The airborne radar survey was much more extensive than the previous on-the-ground measurements of 2005 (Fig. 4a). The numerous surveyed tracks included almost the whole volcanic edifice excluding the steepest western flanks, where the helicopter experienced turbulence and could not follow the previously designed tracks. On the eastern side, most of the tracks followed the main flow lines from the top of the cone down to Glaciar Pichillancahue-Turbio main tongues. Also, several tracks were performed perpendicular to the main flow lines, in order to obtain more complete data coverage and crossing points for validation and comparison purposes.

In general, there is a good agreement in the overlapping values at the 169 radar crossing points, without any spatial or directional orientation bias. When analysing the differences to determine the precision of the measurements, the mean and standard deviation equated to 3.3 and 4.4 m, respectively.

Each data point of the radar profile (Fig. 4a orange line), and the resulting radargram along this profile (e.g. Fig. 4b), is a compilation of radar traces recorded every few metres along the flown track. These traces are stacked together, where the x -axis is the surveyed distance along the track and the y -axis is the travel time (in μs) of the return wave (left side of Fig. 4b) and the derived ice thickness (in km at the right side of Fig. 4b). This radargram was already geo-located, migrated and gain adjusted in order to help the interpretation of the subglacial returns. In this profile (Fig. 4b), most of the subglacial returns are clear, apart from the segments at $x = 1,600$ and $x = 3,000$ – $4,000$, where the subglacial topography looks noisy, probably due to the effects of crevasses or debris-covered layers that

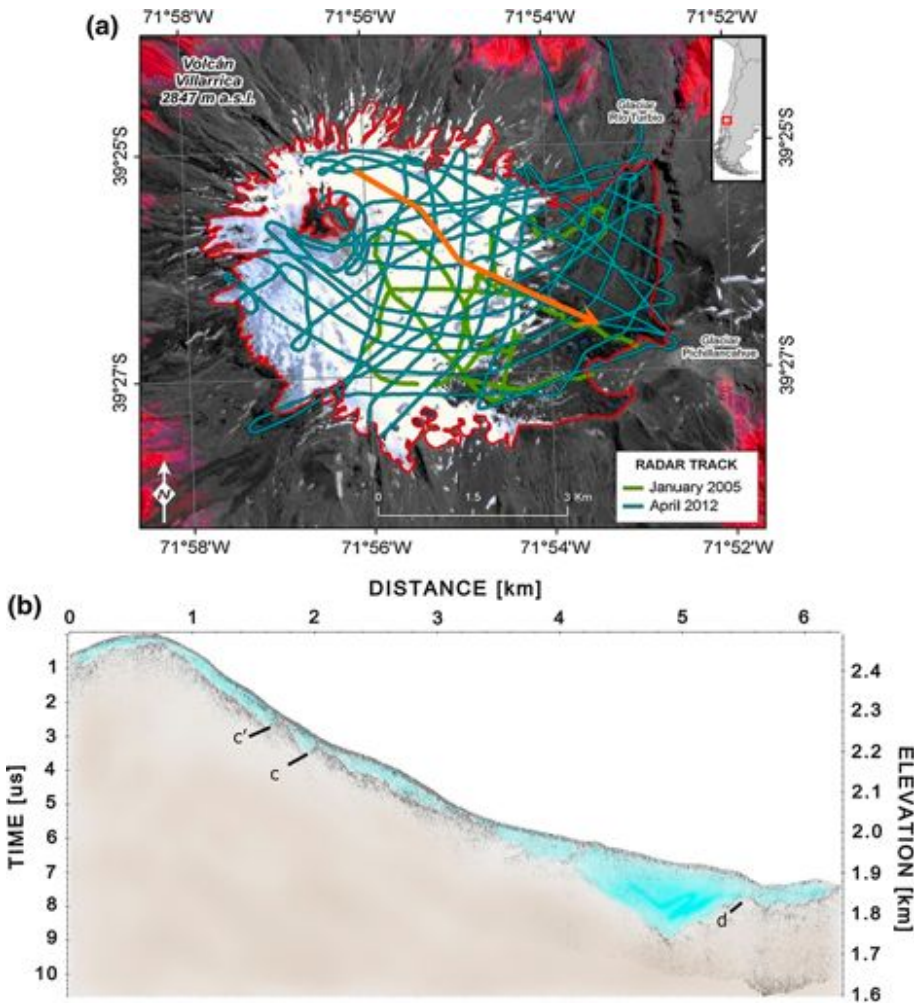


Fig. 4 **a** Radar tracks surveyed on the ground in 2005 (Rivera et al. 2006) and during the airborne survey of January 2012. The background is a false colour composite ASTER acquired in February 26, 2011. In orange, the profile showed below. **b** The radargram shows in light blue the ice thickness. Letters *c*, *c'* and *d* are discussed in the text

perturb the radar wave propagation, and in some cases, completely prevents radar wave ice penetration.

Most of the internal layers within the radar data are isochronous, and in places where the ice flows over abrupt subglacial topographies or nunataks, the layers can be forced upward (see at $x = 4000$ in Figure 4b), until the englacial sediments reach the surface, at the thrust angle associated with the degree of compressive ice flow (Rivera et al. 2013). At Volcán Villarrica, this type of upward layering is associated with pyroclastic material (pyroclastic and epiclastic material, including lapilli and coarse scoriaceous ashes and minor pumiceous) visible all along the ablation area of Glaciar Pichillancahue-Turbio. These materials were most likely originally deposited on top of the glacier during the large Pucón

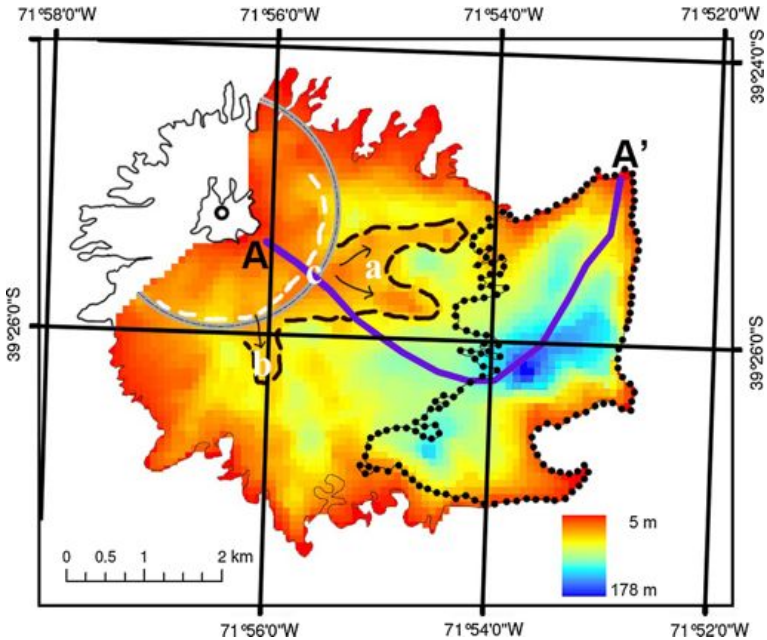


Fig. 5 Ice thickness DEM (m). In *light grey* and letter *c* (see in Fig. 4) are indicated the approximate location of the inner caldera (Caldera 3 in Moreno and Clavero (2006)). *Dotted line* indicates the debris-covered ice area in 2011. *Purple line* indicates profile A–A' showed in Fig. 6. Letters *a* and *b* are possible subglacial lava tongues (*dashed black and arrows*) described in the text. The *dashed white line* represents possible ring faults or collapsed scarps

Ignimbrite eruption that occurred ca. 3,700 years BP (Clavero and Moreno 2004; Silva et al. 2010) and were then progressively covered by snow and ice. Becoming incorporated into the ice flow these layers now emerge at the ablation area.

All the radar data obtained in the 2012 survey, plus some adjusted data collected in 2005 from areas without airborne survey coverage, were interpolated to produce an ice thickness DEM (Fig. 5). The thickness model shows that the deepest ice (near 190 m) is present in areas of Glaciar Turbio's ablation zone (Figs. 5 and 6), where the slope of the surface topography is smooth. As expected, the steepest cone has thinner ice and additionally there is a ring of shallow ice approximately where the young summit caldera (letter *c* in Figs. 5 and 6) has been suggested to be located (Clavero and Moreno 2004).

Thanks to the resulting subglacial topography, plus the surface topography, a manual delineation of glacier basins resulted in 9 basins, associated with a similar number of lahar channels downstream (Table 4). The maximum w.eq. volume was detected at the Turbio basin (Number 1 in Fig. 7), which is consistently the origin of lahars that flowed down in the XXth Century eruptions of 1904, 1908, 1920, 1948 and 1971 along the Ríos Pedregoso and Turbio toward the Lago Villarrica. However, today one of the basins with higher hazards associated with lahars, considering the lahar channels proximity to potentially affected populated areas (Coñaripe), is Diuco (Number 3 in Fig. 7), where a total volume of 0.18 km³ w.eq. is stored. From this basin, a 4,000 to 8,000 m³/s peak discharge lahar was generated in March 1964, resulting in 25 casualties (Naranjo and Moreno 2004).

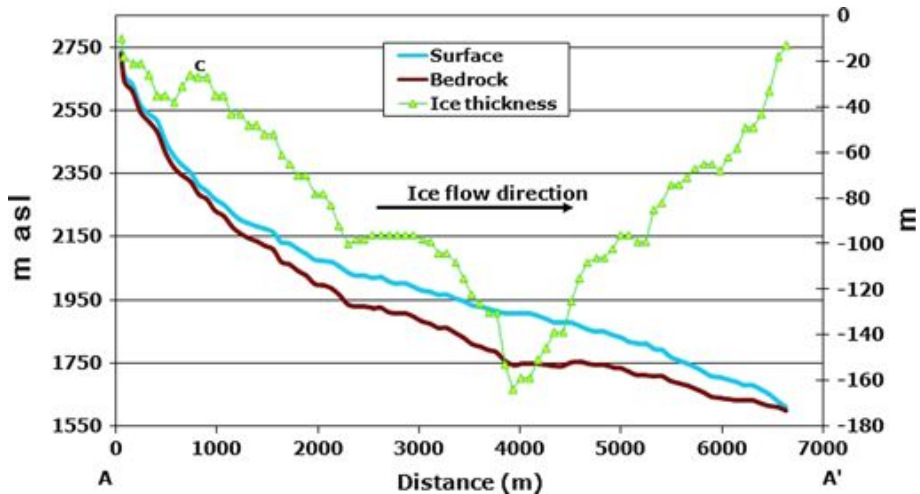


Fig. 6 Surface and subglacial topography (m asl) and ice thickness (m) along profile A-A'. Location of the profile and letter *c* are shown in Fig. 5

3.4 Geological feature in the subglacial topography

Thanks to the resulting subglacial topography, in the topographic profile shown in Fig. 4b, it is possible to observe 3 main subglacial topographic features, representing topographic highs that could be associated with the rim structures of the volcanos calderas. Topographic highs marked *c* and *c'* in Fig. 4b, are located where the youngest caldera rim has been interpreted to be, suggesting that they could represent ring faults or collapsed scarps (marked with dashed white and grey lines in Fig. 5). Two of the possibly collapsed blocks coming from this rim can be observed in Fig. 5 (arrows). These blocks suggests that the collapse that took place 3.7 ka ago forming the Pucón eruption (Clavero and Moreno 2004; Silva et al. 2010), formed several ring structures. Towards the east on the same profile (Fig. 4b), one main topographic high marked *d* on the figure can be observed. This is located close, but several hundreds of meters towards the West, of what has been interpreted to be the surface expression of the main structure of the old nested caldera dated at 13.7 ka.

The resulting subglacial topography shows other features that could be related to the Late Pleistocene-Holocene eruptive history of the volcano. For example, it is possible to observe that from the main cone built on the Northwestern side of the major caldera, two “tongues” developed towards the east (marked *a* in Figure 5) and one towards the South (marked *b* in Fig. 5). These tongues probably represent lava flows that have surpassed the rim of the Holocene caldera structure, which formed ca. 3.7 ka ago (Clavero and Moreno 2004).

Another interesting feature is a subglacial topographic high, marked with a grey line in Fig. 5 and with a *c* in Fig. 6, which probably represents the rim of the youngest caldera, associated with the most recent major eruptive event at Volcán Villarrica, the Pucón Ignimbrite (Clavero and Moreno 2004). This feature is located in a very similar place as the one suggested previously by other authors based only on surface expressions (e.g. Moreno and Clavero 2006). Finally, a deep depression can be observed in Fig. 5, developed on the Eastern side of the caldera (deep ice area shown in blue colours), suggesting

Table 4 Glacier basins from where lahars are generated at Volcan Villarrica (see Figs. 1 and 7 for location). s/d are basins without enough ice thickness data

| Basin ID | Name of Lahar flow | Area (km ²) | AAR (%) | Altitude range (m asl) | | Ice thickness (m) | | Volume (km ³ w.eq.) |
|----------|--------------------|-------------------------|---------|------------------------|-------|-------------------|------|--------------------------------|
| | | | | Min | Max | Max | Mean | |
| 1 | Turbio | 11.7 | 49 | 1,581 | 2,751 | 168 | 57 | 0.54 |
| 2 | Palguín | 6.7 | 46 | 1,789 | 2,686 | 186 | 67 | 0.36 |
| 3 | Diuco | 5.3 | 75 | 1,795 | 2,816 | 94 | 43 | 0.18 |
| 4 | Chaillupén | 1.1 | 68 | 1,866 | 2,762 | 50 | 24 | 0.021 |
| 5 | Voipir | 1.9 | 90 | 1,854 | 2,720 | 46 | 24* | 0.04 |
| 6 | Huichatio | 0.2 | 100 | 2,074 | 2,586 | s/d | 24* | 0.004 |
| 7 | Molco | 0.4 | 96 | 1,955 | 2,605 | s/d | 24* | 0.007 |
| 8 | Correntoso | 0.6 | 100 | 2,047 | 2,700 | s/d | 24* | 0.012 |
| 9 | Zanjón Seco | 0.4 | 100 | 2,023 | 2,749 | 42 | 24* | 0.007 |
| | Total (2011) | 28.3 | 59 | 1,581 | 2,816 | 186 | 50** | 1.17 |

AAR Accumulation Area Ratio

* indicates a unique value assigned to these basins, based upon the mean value of a nearby basin with data (N 4). ** is the mean ice thickness of all the available data in the resulting DEM

that flows younger than 13.7 ka have not been able to fill completely that area of the collapse structure, and therefore have been confined to areas closer to the active cone formed after that collapse.

4 Discussion

The climate signals observed in the region in recent decades, indicate a reduction in precipitation (Carrasco et al. 2008), a warming cycle of air temperatures, especially at high altitude where the glaciers are located (Falvey and Garreaud 2009), and an upward migration of the snowlines (Carrasco et al. 2005). These conditions are resulting in generalized smaller snow accumulation rates, explaining glacier area reductions and ice thinning.

Volcán Villarrica glaciers are not an exception to this shrinking trend, as its negative glacier area change rate since 1961 is similar or slightly smaller than the majority of the observed glacier reductions at the Southern Andes, including both, glaciers on volcanoes, and on non-volcanic mountains (Rivera and Bown 2013). This relatively smaller area reduction could be related to the occurrence of a large debris-covered ablation area. This debris coverage reduces the ablation of the underlying ice, due to the insulation properties of the pyroclasts (lapilli and coarse ash) and other volcanic materials (Brock et al. 2007).

The most important area reduction at the volcano took place at Glaciar Pichillancahue-Turbio (Fig. 2), where the AAR is the smallest (near 49 %, Table 4), and as result, the warming trend is probably inducing higher ablation. The other basins have higher AARs, meaning that the accumulation areas are predominant, and therefore the glacier sensitivity to temperature changes is smaller.

The ice elevation changes observed at the volcano are in the lower bound of the thinning rate range observed in Patagonia (Rignot et al. 2003). Unfortunately, no other ice elevation changes are available from glaciers within this region apart from the previous estimations available at Villarrica, showing similar thinning rates (Rivera et al. 2006).

The ice thicknesses obtained at the volcano are within the previously measured range (between 50 and 195 m), however the mean thickness (Table 4) is much smaller than estimated before. This is mainly explained by the spatially more representative data obtained in 2012, when the survey included the deepest parts as well as the steepest glacier slopes, where the ice is normally thinner. This more comprehensive data set allows for estimation of a more accurate and precise equivalent volume of water at the volcano.

The total volume w.eq. store as snow and ice at the volcano was first estimated at 6.4 km^3 (Rivera 1989). This was obtained using a function between glacier area (39.9 km^2 in 1961) and mean ice thickness (200 m) and a mean density of 0.8 gr/cm^3 . This relation was originally defined for Norwegian glaciers by Ostrem and Ziegler (1969). Following this, a total volume of 6.5 km^3 w.eq. was estimated by Naranjo and Moreno (2004), based on crevasse depth estimations. In recent years, using limited but more precise on-the-ground ice thickness data, Rivera et al. (2006) calculated a total volume of 2.3 km^3 w.eq. at the volcano in 2005. Using the most recent data collected in the area in 2012 the water equivalent volume at the volcano is estimated at 1.17 km^3 with an estimated error of 10 %, mainly attributed to the uncertainties of the ice thickness DEM.

Interestingly when the more precise 2012 volume data is compared to estimations obtained by global ice thickness models, the results are quite different. For example, Grinsted (2013) proposed two functions for glaciers bigger than 25 km^2 of ice (Eqs. 1 and

2), and the following functions (Eqs. 3 and 4) for glaciers smaller than 25 km², where *V*: Volume of water equivalent in km³; *A*: area in km² and *R*: elevation range in km.

$$V = 0.0746R^{0.175}A^{1.16} \tag{1}$$

$$V = 0.0540A^{1.2} \tag{2}$$

$$V = 0.0385R^{0.2}A^{1.29} \tag{3}$$

$$V = 0.0435A^{1.23} \tag{4}$$

Applying these equations to the total glacier area of Volcán Villarrica, without distinction between basins, the results (Table 5) for each equation are 3.74 and 2.98 km³, respectively. This overestimation (3–4 times our results), indicates high uncertainties when models are based upon restricted on-the-ground validation data. However, when the glacier is divided between main basins, the comparison with global equations for glaciers smaller than 25 km² is much closer (shown in Table 5), only 60 % higher with Eqs. (3) and (4) versus our results.

This overestimation could be due to the rough and steep surface topographic relief on a volcanic cone such as Villarrica, on which the elevation range is more than 1.2 km, and/or because the volcanic cone subglacial topographic is irregular, due to the existence of a complex caldera depression formed by at least two nested calderas (Clavero and Moreno 2004).

If the mean ice thickness obtained at Volcán Villarrica (50 m) is compared to Andean regional estimations (Eq. 5) by Huss and Farinotti (2012), where *h*: mean ice thickness in m; *A*: glacier area in m²

$$h = 0.310A^{0.327} \tag{5}$$

the result (Table 5) is 50 % higher (85 m), confirming the general overestimation of the parameters used for determining glacier volume storage on mountain glaciers.

To estimate the water equivalent volume change for the whole volcano, the historical data described above was re-assessed. Since 1961, the ice elevation change has been -0.95 ± 0.36 m/a. Taking into account a mean ice thickness of 50 m, estimated with the most recent data set (2012), the water equivalent volume in 1961 was 3.14 ± 0.7 km³, which compared to the most recent data, results in a total volume loss of 63 ± 10 % w.eq. in the last 51 years. This volume reduction is mainly explained by high thinning rates affecting both the accumulation and ablation areas. Area reductions are also an important factor, especially for the main frontal tongue of Glaciar Pichillancahue-Turbio (Rivera et al. 2012) and at the northern flank of the volcano, where the 1971 and 1984 eruptions destroyed part of the glaciers and eroded channels between 20 and 60 m deep into the ice (González-Ferrán 1995; Naranjo and Moreno 2004).

In order to estimate the load effect on the volcanic edifice of the w.eq. volume calculated here, an important amount of temporal snow volume must be added, however, very little snow accumulation or meteorological data are locally available (Brock et al. 2012). To solve this problem, the data collected at the previously described Temuco Maquehue airfield station was used. This station is one of the oldest and best maintained in the region, having a climatological (1961–1990) mean annual precipitation of 1,157 mm (DMC 1991). Based upon these data, and considering a regional precipitation gradient of 200 mm/100 m (DGA 1987), a mean annual precipitation of 4930 mm at 2000 m asl on Volcán Villarrica

Table 5 Ice thickness and volume of water equivalent estimated by this study versus the results obtained by the application of the equations described in the text

| Basin | Area (km ²) | Altitude range (m) | Ice thickness (m) | | Volume (km ³ w.eq.) | | | | |
|-------|-------------------------|--------------------|-------------------|-------|--------------------------------|----------------------|-------|----------------------|-------|
| | | | This study | Eq. 5 | This study | For glacier areas | | For glacier areas | |
| | | | | | | > 25 km ² | | < 25 km ² | |
| | | | | | | Eq. 1 | Eq. 2 | Eq. 3 | Eq. 4 |
| 1 | 11.7 | 1,170 | 57 | 63 | 0.54 | | 0.95 | 0.90 | |
| 2 | 6.7 | 897 | 67 | 53 | 0.36 | | 0.44 | 0.45 | |
| 3 | 5.3 | 1,021 | 43 | 49 | 0.18 | | 0.33 | 0.34 | |
| 4 | 1.1 | 896 | 24 | 29 | 0.021 | | 0.04 | 0.05 | |
| 5 | 1.9 | 866 | 24 | 35 | 0.04 | | 0.09 | 0.10 | |
| 6 | 0.2 | 512 | 24 | 17 | 0.004 | | 0.00 | 0.01 | |
| 7 | 0.4 | 650 | 24 | 21 | 0.007 | | 0.01 | 0.01 | |
| 8 | 0.6 | 653 | 24 | 24 | 0.012 | | 0.02 | 0.02 | |
| 9 | 0.4 | 726 | 24 | 21 | 0.007 | | 0.01 | 0.01 | |
| | ∑ | | | | ∑ | | ∑ | ∑ | |
| Total | 28.3 | 1,235* | 50* | 85* | 1.17 | 3.74* | 2.98* | 1.89 | 1.89 |

* Values calculated for the total glacier area (no basins used)

was estimated. Considering the above, we estimated that during every autumn-winter season a mean temporal snow accumulation of near 10 m is added to the volcano (approximately 0.14 km³ or 140 × 106 ton). The removal of this yearly added temporal load can be related to the frequent beginning of eruptive processes in spring, that has been observed in historical times (Petit-Breuihl and Lobato 1994). This load effect is also accompanied by the fact that meltwater infiltration into the upper part of the volcanic system increases in springtime, process that could also favour the occurrence of eruptive events through phreatomagmatic explosions near the crater, or other mechanisms, as observed for example in Icelandic subglacial volcanoes (Albino et al. 2010). This total weight, and the possible load and water infiltration effects, must be considered with care, because it can change annually depending on the amount of snowfall, the altitude of the 0 °C isotherm and the glacier mass balance.

The total water equivalent volume amount at the volcano is one of the main inputs for defining possible resulting lahar volumes to be generated during eruptions and then for modelling lahar inundation areas using different softwares, such as LAHARZ software (Schilling 1998) or the MSF code (Modifies Single Flow, Huggel et al. 2003). In general, eruption-triggered lahar generation and the resulting volumes of such flows depend mainly on the water availability on the volcano (through ice and/or snow cover and therefore on the resulting flow volume) and the effusion rate of the eruption, whether it is an explosive one like in 1948, or an effusive one like in 1971 and 1984. Water availability in an edifice such as Volcán Villarrica is directly related both to the ice thickness in the different basins and to the location of the magma extrusion (explosive and/or effusive), and therefore lahar flows of different volumes are expected to be generated in the valleys surrounding the volcano, as has occurred historically.

The new data presented here suggests that the volume of water eq. available for future lahar generations is smaller than previously thought. Although this could be a positive

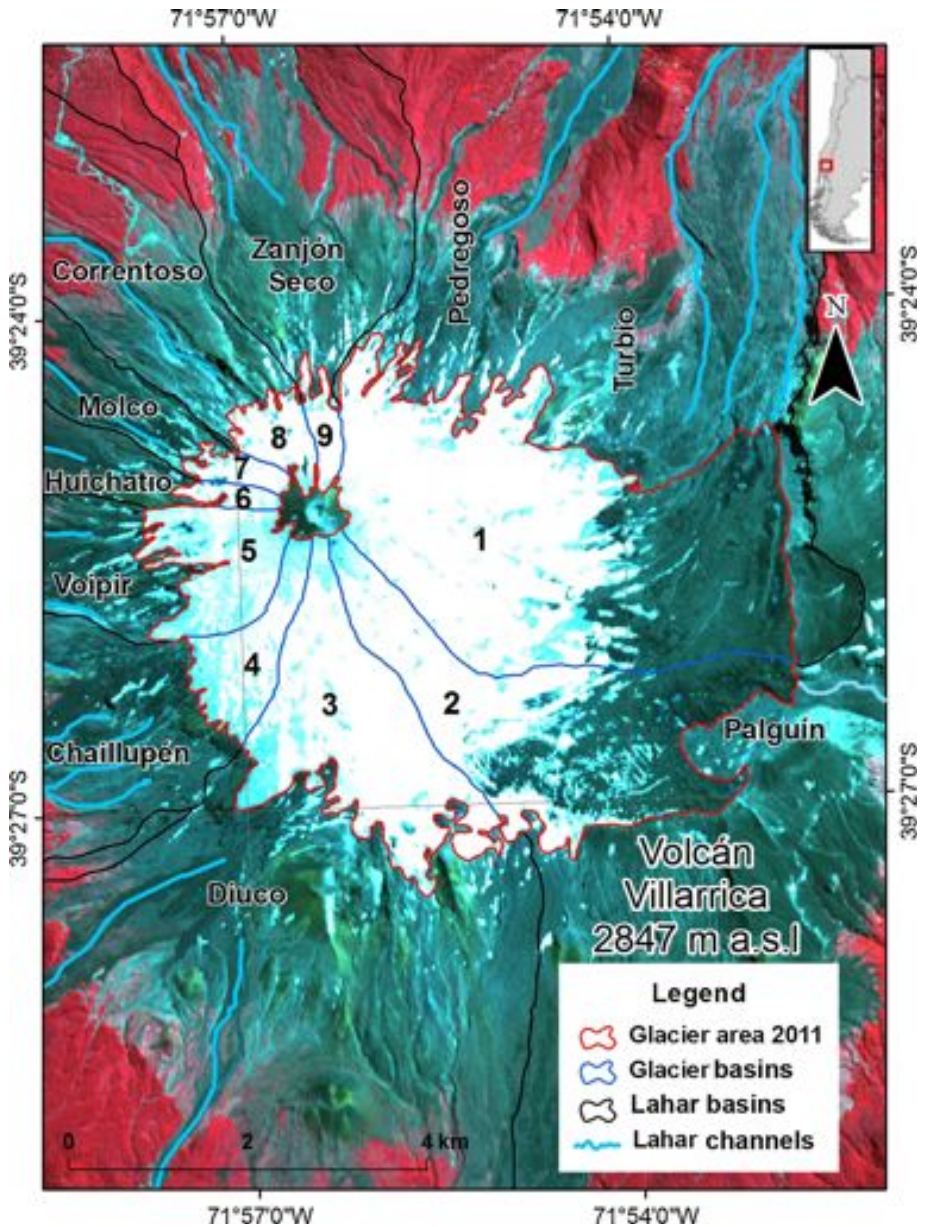


Fig. 7 Glacier basins defined from the main lahars channels around the volcanic cone. Numbers are described in Table 4

effect, the increasing extension of populated areas, especially in areas that have been affected in historical times by lahar flows, still poses an important risk associated with lahars as has been modelled recently (Castruccio 2008; Castruccio et al. 2010). This is for instance the case of the Diuco, Correntoso and Zanjón Seco channels (Numbers 3, 8 and 9 respectively in Fig. 7).

Although lahar flow in the future may be of lower volumes than in the past, the water eq. availability at the upper flanks of the volcano is still high enough to generate destructive lahar flows. More detailed modelling, using both LAHARZ and MSF software, is currently under way (Castruccio, pers. comm., 2014) to better determine the areas that could be affected by lahars of different volumes in the main valleys descending from the volcano. Preliminary results of these models show that important inhabited areas surrounding the active cone will probably be inundated by lahar flows during future eruptive events. Therefore, the data presented here will not only improve lahar modelling for Volcán Villarrica but will also help local authorities to develop better and improved risk management strategies for future volcanic eruptions.

5 Conclusions

The first airborne surveys using LIDAR and Radar systems for Volcán Villarrica glaciers are presented. The resulting new surface topography DEM covered near 50 % of the glacier area on the volcanic cone with a pixel size of 5 m and an accuracy of 0.5 m. The radar survey covered near 88 % of the total glacier area at a 90 m pixel size, where a maximum ice thickness of 191 ± 10 m was measured and a mean thickness for the whole glacier area was estimated to be 50 ± 3 m. Using all the available data it was possible to determine a total volume of water equivalent storage at the volcano of 1.17 ± 0.07 km³ in 2012. The comparison with the previous volumetric data, which was re-processed using the most accurate surface and subglacial topography, determined a volume loss of 63 ± 10 % in the last 51 years. This could be explained by an area shrinkage of 11.61 km² and a mean ice thinning of 0.95 ± 0.36 m/a between 1961 and 2012. Since this thinning rate was only estimated using elevation data obtained in the lower reaches of the glacier in 1961, it must be considered as an upper limit of the long term real value. In recent years (since 2005) the thinning rate increased to 1.03 ± 0.1 m/a.

The volume of ice calculated in this study is much smaller than previous estimations, not only due to the changes observed on the glacier, but also because old estimates lacked accurate ice thickness data. The same could be said for the temporal snow cover layer and corresponding load weight on the volcanic edifice. In order to improve this estimation, a mass balance program using a glaciological method could be useful, but the problem is the crevassed surface of the glacier, precluding on-the-ground operations during most of the year at the accumulation area. Another possibility for improving our knowledge about temporal snow accumulation is the installation of automatic weather stations, including measurements of precipitation and all the energy balance variables. This was tried by CECs a few years ago, but the inclement weather conditions prevailing during the winter destroyed the station structures, sensors and photographic cameras.

The resulting total volume was divided among the main basins from where the lahars have been generated in historical times, allowing for assessment of the glacio-volcanic risks for the population living nearby or along the lahars paths. Fortunately, the basin with maximum w.eq. volume is not the most dangerous in terms of the potentially affected population, however, the nearby infrastructure could be severely damaged if lahar flows are generated there (Turbio, in Fig. 7). The most risky basin has a total volume of 0.18 km³ w.eq. (Diuco, in Fig. 7). This basin experienced a lahar in 1964 that killed more than 20 people when the small town of Coñaripe was partially destroyed. Although the water equivalent availability, better estimated here, could suggest smaller volumes for

future lahars, this does not mean a lower risk associated with this type of volcanic related flows, especially due to the fact that the surroundings of Volcán Villarrica have experienced an important increase in populated areas in recent years. Between 2002 and 2012, the Chilean National Institute of Statistics (INE) estimated an increase of near 58 % of the Pucón county population, including higher densification within the city and more population in the country side areas. This means that the new ice volume assessment will be useful for modelling possible lahar fluxes in this part of the volcano, information already provided to authorities interested in local emergency planning.

Acknowledgments Maximiliano Fuentealba conducted the LIDAR surveys. Norbert Blindow, Gino Casassa, David Ulloa and the private company Unmanned, collaborated in the design and build of the radar. Guisella Gacitúa helped with radar data. Thanks to CONAF for giving the permissions to work in the Villarrica National Park. The research reported here has been supported by FONDECYT 1090387 and Centro de Estudios Científicos (CECs). CECs is funded by the Basal fund of Conicyt among other grants. The transmitter was designed and built in the Federal Institute for Geosciences and Natural Resources (BGR) of Germany. The transmitter was partially funded by the University of California (Irvine). Andrés Rivera is a Guggenheim fellow.

Open Access This article is distributed under the terms of the Creative Commons Attribution License which permits any use, distribution, and reproduction in any medium, provided the original author(s) and the source are credited.

References

- Albino F, Pinel V, Sigmundsson F (2010) Influence of surface load variations on eruption likelihood: application to two Icelandic subglacial volcanoes, Grímsvötn and Katla. *Geophys J Int* 181(10):1510–1524. doi:10.1111/j.1365-246X.2010.04603.x
- Brock B, Rivera A, Casassa G, Bown F, Acuña C (2007) The surface energy balance of an active ice-covered volcano: Villarrica Volcano, southern Chile. *Ann Glaciol* 45(1):104–114
- Brock BW, Burger F, Rivera A, Montecinos A (2012) A fifty year record of winter glacier melt events in southern Chile, 3842S. *Environ Res Lett* 7(4):045,403
- Calder ES, Harris AJ, Peña P, Pilger E, Flynn LP, Fuentealba G, Moreno H (2004) Combined thermal and seismic analysis of the Villarrica volcano lava lake. *Chile. Rev Geol Chile* 31(2):259–272
- Carrasco JF, Casassa G, Quintana J (2005) Changes of the 0C isotherm and the equilibrium line altitude in central Chile during the last quarter of the 20th century. *Hydrol Sci J* 50(6):933–948
- Carrasco JF, Osorio R, Casassa G (2008) Secular trend of the equilibrium-line altitude on the western side of the southern Andes, derived from radiosonde and surface observations. *J Glaciol* 54(186):538–550
- Casassa G (1987) Ice thickness deduced from gravity anomalies on Soler Glacier, Nef Glacier and The Northern Patagonia Icefield. *Bull Glacier Res* 4:43–57
- Casassa G, Acuña C, Zamora R, Schliermann E, Rivera A (2004) Ice thickness and glacier retreat at Villarrica Volcano. In: Lara L, Clavero J (eds) *Villarrica Volcano (39.5S)*, Southern Andes, Chile. Servicio Nacional de Geología, Santiago, Chile, pp 53–60
- Castruccio A (2008) Comparación y Modelación numérica de lahares calientes en el volcán Calbuco (41,3S) y lahares fríos en el volcán Villarrica (39,5S), Andes Del Sur. Tesis para optar al grado de Magister en Ciencias, mención Geología. PhD thesis, Universidad de Chile
- Castruccio A, Clavero J, Rivera A (2010) Comparative study of lahars generated by the 1961 and 1971 eruptions of Calbuco and Villarrica volcanoes, Southern Andes of Chile. *J Volcanol Geotherm Res* 190(3–4):297–311
- Clavero J, Moreno H (2004) Evolution of Villarrica Volcano. In: Lara L, Clavero J (eds) *Villarrica Volcano (39.5S)*, Southern Andes, Chile. Servicio Nacional de Geología, Santiago, Chile, pp 17–27
- DGA (1987) Balance Hídrico de Chile. Dirección General de Aguas, Ministerio de Obras Públicas. Tech. rep., Dirección General de Aguas, Santiago, Chile
- DMC (1991) Normales climatológicas 1961–1990. Fuerza Aérea de Chile. Tech. rep., Dirección Meteorológica de Chile, Santiago, Chile

- Falvey M, Garreaud RD (2009) Regional cooling in a warming world: Recent temperature trends in the southeast Pacific and along the west coast of subtropical South America (1979/2006). *Journal of Geophysical Research* 114(D4):1–16
- Gilbert JS, Stasiuk MV, Lane SJ, Adam CR, Murphy MD, Sparks RSJ, Naranjo JA (1996) Non-explosive, constructional evolution of the ice-filled caldera at Volcán Sollipulli, Chile. *Bull Volcanol* 58(1):67–83
- González-Ferrán O (1995) Volcanes de Chile. Instituto Geográfico Militar, Santiago, Chile
- Grinsted A (2013) An estimate of global glacier volume. *Cryosphere* 7(1):141–151
- Huggel C, Kääb A, Haeblerli W, Krummenacher B (2003) Regional-scale GIS-models for assessment of hazards from glacier lake outbursts: evaluation and application in the Swiss Alps. *Nat Hazards Earth Syst Sci* 3(6):647–662
- Huss M, Farinotti D (2012) Distributed ice thickness and volume of all glaciers around the globe. *J Geophys Res* 117(F4):F04,010
- Kennett M, Laumann T, Lund L (1993) Helicopter-borne radio-echo sounding of Svartisen, Norway. *Ann Glaciol* 17:23–26
- Lara L (2004) Overview of Villarrica Volcano. In: Lara L, Clavero J (eds) *Villarrica Volcano (39.5S), Southern Andes, Chile*. Servicio Nacional de Geología, Santiago, Chile, pp 5–12
- Macheret Y, Moskalevsky M, Vasilenko E (1993) Velocity of radio waves in glaciers as an indicator of their hydrothermal state, structure and regime. *J Glaciol* 39(132):373–384
- Moreno H (2000) Mapa de Peligros Volcánicos del volcán Villarrica. Documentos de trabajo #17, escala 1:75,000. Tech. rep., Servicio Nacional de Geología y Minería.
- Moreno H, Clavero J (2006) Geología del área del Volcán Villarrica. Serie Geología Básica, Carta Geológica de Chile, No. 98, escala 1:50,000. Tech. rep., Servicio Nacional de Geología y Minería.
- Naranjo J, Moreno H (2004) Laharic debris-flows from Villarrica Volcano. In: Lara L, Clavero J (eds) *Villarrica Volcano (39.5S), Southern Andes, Chile*, Chilean Geol. Survey, Santiago, Chile, pp 28–45.
- Newhall CG, Self S (1982) The volcanic explosivity index (VEI) an estimate of explosive magnitude for historical volcanism. *J Geophys Res* 87(C2):1231
- Ostrem G, Ziegler T (1969) Atlas Over Breer I Sor-Norge: Atlas of Glaciers in South Norway. Norges Vassdrags-og Elektrisitetsvesen, Oslo
- Paterson W (1994) *The physics of glaciers*, 3rd edn. Pergamon Press, Great Britain
- Petit-Breuilh M, Lobato J (1994) Análisis comparativo de la cronología eruptiva histórica de los volcanes Llaima y Villarrica. In: *Proceedings of the Congreso Geológico Chileno No. 7, Concepción, Chile*, pp 366–370.
- Rignot E, Rivera A, Casassa G (2003) Contribution of the Patagonia Icefields of South America to sea level rise. *Science (New York, NY)* 302(5644):434–7
- Rivera A (1989) Inventario de glaciares entre las cuencas de los ríos Bio Bio y Petrohué. Su relación con el volcanismo activo: Caso del volcán Lonquimay. PhD thesis, Departamento de Geografía, Universidad de Chile.
- Rivera A, Bown F (2013) Recent glacier variations on active ice capped volcanoes in the Southern Volcanic Zone (37° – 46° S). *Chilean Andes. J S Am Earth Sci* 45:345–356
- Rivera A, Casassa G (2002) Detection of Ice Thickness using radio echo sounding on the Southern Patagonia Icefield. In: Casassa G, Sepúlveda F, Sinclair R (eds) *The Patagonian Icefields. A unique natural laboratory for environmental and climate change studies*. Kluwer Academic/Plenum Publishers, pp 101–115
- Rivera A, Casassa G, Acuña C (2001) Mediciones de espesor en glaciares de Chile centro-sur. *Invest Geogr Chile* 35:67–100
- Rivera A, Bown F, Casassa G, Acuña C, Clavero J (2005) Glacier shrinkage and negative mass balance in the Chilean Lake District (40° S). *Hydrol Sci J* 50(6):963–974
- Rivera A, Bown F, Mella R, Wendt J, Casassa G, Acuña C, Rignot E, Clavero J, Brock B (2006) Ice volumetric changes on active volcanoes in southern Chile. *Ann Glaciol* 43(1):111–122
- Rivera A, Corripio J, Brock B, Clavero J, Wendt J (2008) Monitoring ice capped active Volcán Villarrica in Southern Chile by means of terrestrial photography combined with automatic weather stations and GPS. *J Glaciol* 54(188):920–930
- Rivera A, Cawkwell F, Rada R, Bravo C (2011) Hypsometry. In: Singh V, Singh P, Haritashya U (eds) *Encyclopedia of snow ice and glaciers*. Springer, The Netherlands, pp 551–554
- Rivera A, Bown F, Carrión D, Zenteno P (2012) Glacier responses to recent volcanic activity in Southern Chile. *Environ Res Lett* 7(1):014,036
- Rivera A, Cawkwell F, Wendt A, Zamora R (2013) Mapping blue ice areas and crevasses in west Antarctica using ASTER images, GPS and radar. In: Kargel J, Leonard G, Bishop M, Kaab A, Raup B (eds) *Global land Ice measurements from space*, Springer-Praxis, chap 33.
- Sandmeier K (2004) *Reflexw. Manual version 5*.

- Schilling S (1998) LAHARZ: GIS programs for automated mapping of lahar-inundation hazard zones. USGS report. Tech. rep, USGS, USA
- Schloeder C, Zimmerman N, Jacobs M (2001) Comparison of Methods for Interpolating Soil Properties Using Limited Data. *Soil Sci Soc Am J* 65(2):470
- Silva C, Druitt TH, Robin C, Moreno H, Naranjo JA (2010) The Holocene Pucón eruption of Volcán Villarrica, Chile: deposit architecture and eruption chronology. *Bull Volcanol* 72(6):677–692
- Stern C (2004) Active Andean volcanism: its geologic and tectonic setting. *Rev Geol Chile* 31(2):161–206
- Stern C, Moreno H, López-Escobar L, Clavero J, Lara L, Naranjo J, Parada M, Skewes M (2007) Chilean volcanoes. In: Moreno E, Gibbons W (eds) *The geology of Chile*, Geologic Society of London Press, London, UK, chap 5, pp 149–180.
- Watts R, England A (1976) Radio-echo sounding of temperate glaciers: ice properties and sounder design criteria. *J Glaciol* 17(75):39–48
- Watts R, Wright D (1981) System for measuring thickness of temperate and polar ice from the ground or from the air. *J Glaciol* 27(97):459–469
- Witter J, Delmelle P (2004) Acid gas hazards in the crater of Villarrica volcano (Chile). *Rev Geol Chile* 31(2):273–277
- Zamora R, Ulloa D, Garcia G, Mella R, Uribe J, Wendt J, Rivera A, Gacitúa G, Casassa G (2009) Airborne radar sounder for temperate ice: initial results from Patagonia. *J Glaciol* 55(191):507–512